

A01-16502



**AIAA 2001-0649**  
**A Far-Field Repetitive Pulse Laser Thruster**

Kouichi Mori, Kimiya Komurasaki, Hiroshi Katsurayama,  
and Yoshihiro Arakawa

University of Tokyo, Tokyo, Japan

**39th AIAA Aerospace Sciences Meeting & Exhibit**

**8–11 January 2001**

**Reno, Nevada**

AIAA-2001-0649

## A FAR-FIELD REPETITIVE PULSE LASER THRUSTER

Kouichi MORI\*, Kimiya KOMURASAKI†, Hiroshi KATSURAYAMA‡ and Yoshihiro ARAKAWA§  
 University of Tokyo, Hongo 7-3-1, Bunkyo, Tokyo 113-8656, Japan

## Abstract

The pressure wave expansion around a laser-induced plasma was investigated by experiments and numerical simulations as part of the on-going research of repetitive-pulse laser thrusters. In the experiments, pressure fields around the plasma called a "fire-ball" were measured. The thrust impulse was numerically estimated from the measured pressure profiles assuming a simple fire-ball expansion. As a result, a maximum impulse of 1.1mNs was obtained by a pressure-receiver located at 21 mm apart from the center of expansion with an input energy of 1J. Since this optimum receiver location is far enough from the fire-ball, the heat conduction to the receiver can be neglected in a so-called "far-field thruster."

## INTRODUCTION

In the future, air-breathing repetitive-pulse laser propulsion will serve as an alternative propulsion system for both ground-to-orbit launches and orbit transfers. Recently, Myrabo carried out laser propulsion flight tests and numerical simulations with a scale model named Lightcraft.<sup>[1],[2]</sup> (Fig.1a) Their scale model utilizes atmospheric air as the propellant and therefore, since it does not carry a propellant on-board for a lower stage, the payload ratio is improved remarkably.

When a high-power pulsed laser beam is focused into atmospheric air, breakdown occurs near the focus. A spherical plasma, referred as a fire-ball, is then formed and the slowly decaying part of pulse of the laser shot duration is absorbed in the fire-ball. The laser-induced blast wave is generated by the expansion of this fire-ball. The blast wave reflects on the nozzle wall, providing the direct impulse, and such wall can be regarded as a blast wave receiver. This blast wave also expands through the nozzle, resulting in additional impulse. Due to these physical phenomena, the repetitively transmitted laser energy is converted into a repetitive thrust impulse.

In the Lightcraft, the plasma is produced in the vicinity of the receiver surface, since a solid surface lowers the breakdown threshold of laser power intensity. The strong shockwave exerts the impulse on the receiver. Such type of thrusters can be categorized as near-field thrusters. The near-field means the region where the blast wave is accompanied by the expansion of fire-ball. However, the near-field thruster may have two disadvantages. The first one is the damage to the receiver due

to heat conduction from the fire-ball. The second is the one that a large fraction of explosion energy is carried away from the near-field by the outgoing blast wave without exerting the impulse on the receiver.

To overcome these disadvantages, a far-field thruster is investigated here. It is called far-field to indicate the region where the blast wave has decayed to an acoustic wave and is not accompanied by the fire-ball mentioned earlier. Figure 1b shows a schematic of the far-field thruster being modeled herein. A plasma is produced at the center of a hemispherical receiver. The fundamental relations between the impulse on the receiver and the distance from the fire-ball to the receiver have been investigated in what follows.

When the induced blast wave is very strong, the propagation process of blast wave can be analytically solved using a self-similar solution<sup>[3]</sup>. The limit of applicability of this solution is as follows,

$$p_1 \gg \frac{\gamma + 1}{\gamma - 1} p_0 \geq 6 \times p_0. \quad (1)$$

$p_1$  is the pressure behind the shock front,  $p_0$  is the atmospheric pressure,  $\gamma$  is the specific heat ratio. Under the experimental conditions investigated, unfortunately the post-shock pressures in the far-field are only three times as high as atmospheric pressure. Therefore, the self-similar solution cannot be applied.

In conventional spherical symmetric simulations of the explosion, such as a TNT charge explosion, the balloon analogue<sup>[4]</sup> is often used as the source model, in which case the blast wave propagation is initiated by the rupture of a statically pressurized volume<sup>[5]</sup>. Despite the lack of modeling of complex mechanisms such as detonation or deflagration, the computed blast wave propagation process in the far-field can be made to match up to the actual process by the adjustment of balloon conditions keeping a low computational cost.

In this research, similarly to this balloon analogue, the fire-ball encompassed by the blast

\*Graduate student, Department of Advanced Energy

†Associate Professor, Department of Advanced Energy, Member AIAA

‡Graduate student, Department of Aeronautics and Astronautics, Student Member AIAA

§Professor, Department of Aeronautics and Astronautics, Member AIAA

Copyright ©2001 by the American Institute of Aeronautics and Astronautics, Inc. All rights reserved.

wave is assumed homogeneously heated during the laser irradiation. Chemical reactions and detailed laser supported detonation/combustion mechanisms were not incorporated. The measured pressure profiles in the far-field are reproduced by the model, and the thrust impulse is estimated at several receiver locations.

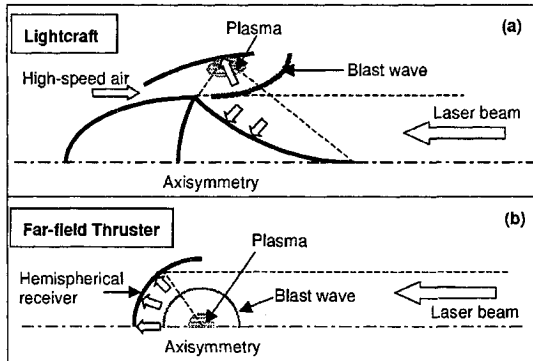


Fig. 1 Lightcraft and Far-field Thruster.

### EXPERIMENTAL SETUP FOR AIR-PLASMA PRODUCTION

An air plasma was produced using a 10-J-pulse TEA CO<sub>2</sub> laser in a quiescent air at standard conditions. The temporal profile of the laser power was measured using a photon-drag CO<sub>2</sub> laser detector (Hamamatsu photonics-B749) as shown in Fig.2. At first, a leading edge spike appears. The peak power of the spike is 12MW with 0.2 $\mu$ s width. Then, a slowly decaying tail follows the spike. The average power of the tail is 2MW with 5 $\mu$ s duration. A cross section of the laser beam is a square of 30mm  $\times$  30mm. Since the transverse mode is a multi-mode, it is difficult to estimate the minimum spot diameter and the intensity at the focus. The laser beam was focused using an off-axial parabola mirror, whose focal length is 19.1mm.

Shadowgraphs were taken to observe the temporal variation of density discontinuities around the plasma. The measurement system is shown in Fig.3. An ICCD camera with a high-speed gating (Oriol Instruments InstaSpec<sup>TM</sup>V ICCD detector, Model77193-5) was employed. The exposure period was 1 $\mu$ s. An optical emission from a gap-switch of a laser discharge tube was utilized to trigger the gate of the camera. The gap-switch emission was detected ahead of the laser irradiation by a photo-sensor through an optical fiber, and the signal was transmitted to a delay-circuit (Stanford Research Systems, Inc. Digital Delay/Pulse Generator Model DG535), enabling photographs to be taken with any delay period from the laser incidence. A He-Ne laser was used as the light source.

A spherical blast wave is driven by a rapid expansion of the laser-produced plasma. It propagates outward and then decays as an acoustic

wave. The decaying process of the blast wave was measured in the far-field using a quartz pressure gauge (Kistler-603B, natural frequency: 400KHz.)

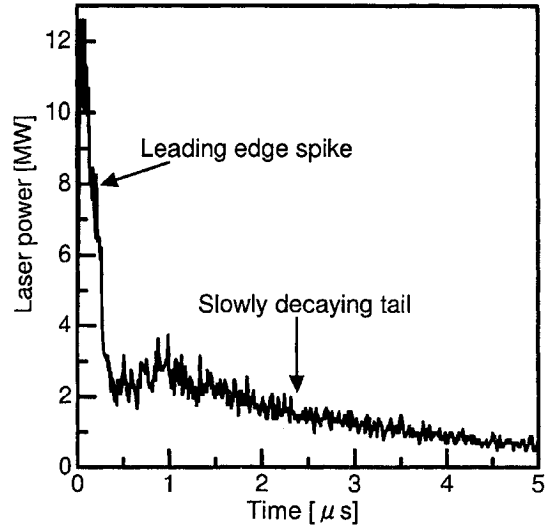


Fig. 2 Temporal profiles of laser power.

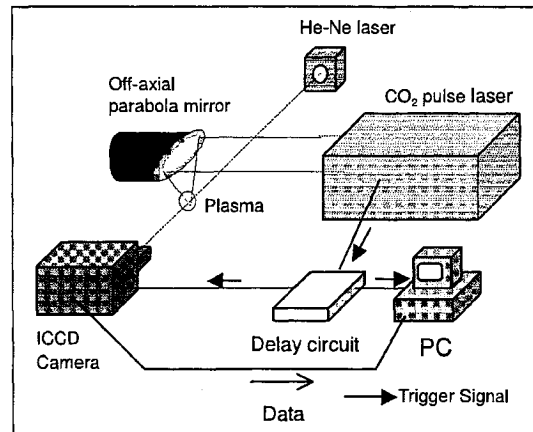


Fig. 3 Schematic of measurement system to obtain shadowgraphs.

### NUMERICAL METHOD

#### Modeling and Governing equations

On the fire-ball surface, the side of laser incidence expands faster than at the other side because the laser energy supports the blast wave. Therefore, the expansion speed of fire-ball practically depends on the laser incident direction. However, the propagation process of the blast wave in the far-field is independent of the laser incident direction, so that the flow field is assumed spherically symmetric and 1-D spherical symmetric Navier-Stokes equations are adopted as the governing equations. The region encompassed by the blast wave is regarded as the fire-ball in which the gas is homogeneously heated during the laser

irradiation ( $0 \sim 5\mu\text{s}$ ). The source term in the energy equation is given as.

$$\dot{s} = \frac{\eta_L P_{\text{laser}}}{4/3\pi R_B^3} \text{ [W/m}^3\text{]} \quad (0 < r < R_B). \quad (2)$$

Here, the measured temporal profile of the laser power,  $P_{\text{laser}}$ , shown in Fig.2 is used.  $R_B$  is the radius of the fire-ball, which is computed at every time-step as the position of shock front during the laser irradiation.  $\eta_L$  is the fraction of incident laser energy that is absorbed in the plasma. Although  $\eta_L$  is intrinsically a function of the density and temperature of plasma,  $\eta_L$  is chosen as a tuning parameter in his study and tuned so as to have the same pressure pulses in the measurements and the computations.

For air in at standard conditions, the breakdown threshold of laser power intensity is  $I_{\text{break}} = 10^{12} \sim 10^{13} \text{ MW/m}^2$  at the  $\text{CO}_2$  laser wavelength of  $10.6\mu\text{m}$ . Breakdown occurs at the spot where the intensity of incident laser beam is equal to this  $I_{\text{break}}$ . An initial fire-ball radius after the breakdown,  $r_{\text{ball}0}$ , is determined as,

$$P_{\text{max}} = \pi r_{\text{ball}0}^2 \times I_{\text{break}} \Rightarrow r_{\text{ball}0} = 0.62 \sim 1.95 \text{ [mm]}. \quad (3)$$

The maximum laser power,  $P_{\text{max}}$ , is 12MW. The initial  $R_B$  is set identical to this  $r_{\text{ball}0}$ . As  $r_{\text{ball}0}$  in the above-mentioned range did not affect the induced flow field in the far-field at all, the  $r_{\text{ball}0}$  was set identical to 1.95mm in this calculation.

#### **Numerical scheme and boundary condition**

A so-called Simple High Resolution Scheme<sup>[6]</sup> is used for the estimation of a numerical flux. The spatial accuracy is increased to the third order by using MUSCL interpolation<sup>[7]</sup>. The time accuracy is increased to the fourth order by using a four-step Runge-Kutta scheme. Calculations are conducted at nine different locations of the receiver. The origin of spherical coordinate is set at the focus. The receiver is placed at  $R_{\text{rec}} = 18\text{mm} \sim 34\text{mm}$  from the focus with the interval 2mm. In all cases, the grid resolution  $\Delta r$  is 0.02mm. On the receiver, the flow is assumed stagnated and the wall temperature is set identical to 300K.

## **RESULT AND DISCUSSION**

### **Experimental Results**

The shadowgraphs are shown in Fig.7. At  $t = 0\mu\text{s}$ , precisely at the beginning of the laser incidence, a strong emission from the plasma is observed. At  $t = 4\mu\text{s}$ , the emission is weakened and a blurry discontinuity is observed. At  $t = 7\mu\text{s}$ , after the laser irradiation takes place, a discontinuity appears in shadowgraph at this time. It propagates outward subsequently. At about  $t = 13\mu\text{s}$ , the discontinuity is split into two discontinuities. The location of these discontinuities are plotted

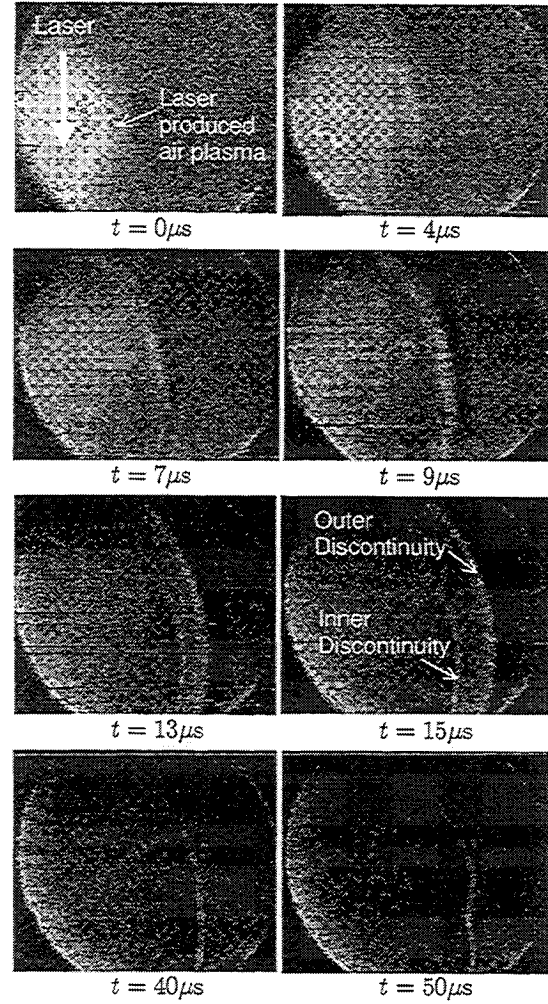


Fig. 7 Shadowgraphs after the laser irradiation.

as a function of time in Fig.8.  $R$  is the distance from the focus. The outer one continues to propagate outward, whereas the inner one stays near at  $R = 12\text{mm}$ . The outer one would be a shock front driven by the expansion of the laser-produced plasma and the inner one a boundary of the laser-produced plasma.

This can be confirmed by comparing these  $(R, t)$  plotted results with the ones obtained using formulas of analytical models. The diagram for inner discontinuity is fitted to the formula of a Drag model<sup>[8]</sup>, which expresses an expanding radius of laser-produced plasma in a non-vacuum atmospheric condition. On the other hand, the diagram for the outer one is fitted to the formula of Sedov solution of the point blast explosion theory<sup>[3]</sup>, which is known as an analytical solution for the propagation of a strong spherical blast wave. The formulas are as follows,

$$R_{\text{inner}} \propto 1 - \exp(-t/\tau) \quad (\text{Dragmodel}) \quad (4)$$

$$R_{\text{outer}} \propto t^{2/5} \quad (\text{Sedovsolution}) \quad (5)$$

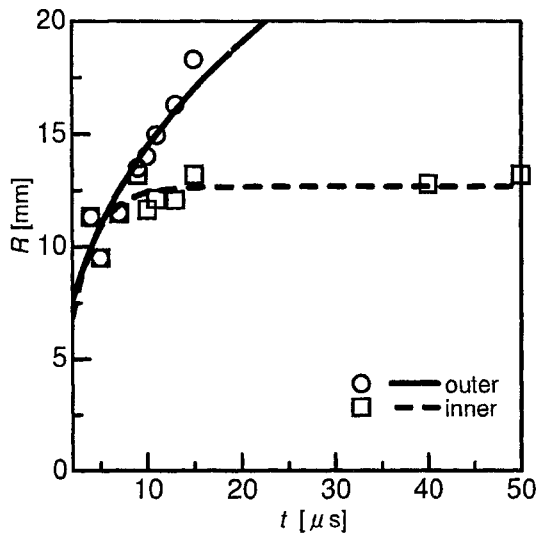


Fig. 8 Position-time plots of the discontinuities.

In the Drag model, the time constant for the decay of the plasma expansion,  $\tau$ , was  $5\mu\text{s}$ , which is same as the duration of the laser pulse. The energy input via laser beam is assumed a driver of the expansion of the heated region against the atmospheric pressure. The expansion pushes the atmosphere out and drives a blast wave into the far-field. The measured plots and theoretical curves are in good agreement as shown in Fig.8

The pressure in the far-field was measured using a pressure gauge. The gauge was put on a wall facing perpendicularly to the direction of the wave propagation and the wall was moved from  $R = 18\text{mm}$  to  $35\text{mm}$ . The measured pressure history at  $R = 20\text{mm}$  is shown in Fig.9. The shock is reflected on the wall, resulting in a sharp spike. Negative gauge pressure is observed in the following part of the pressure pulse. This negative phase is typical of spherical blast waves.

The magnitude of the peak pressure is around  $3\text{atm}$  at  $R = 20\text{mm}$  and decreases as it propagates outward, while the pulse width increases gradually. The shock is too weak to use the point blast explosion theory (a similarity solution) for the analysis of wave propagation.

#### Numerical Results

Figure 10 shows a comparison between measured and computed positive pressure pulses at different locations of receiver. Closed circles indicate the measured values and open circles indicate the computed values. When  $\eta_L$  is 10%, the computed values agree well with the measured values. As a result,  $\eta_L$  is assumed 10% to reproduce the measured pressure waves.

Since the laser transparency measured behind the focus is only 2% in this experiment,  $\eta_L$  was unexpectedly small. There are two possible reasons accounting for this: One is due to the fact that

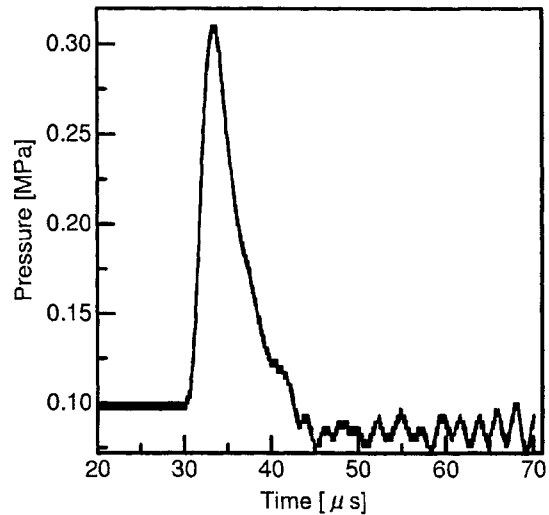


Fig. 9 Temporal variation of the pressure on the wall placed at 20mm.

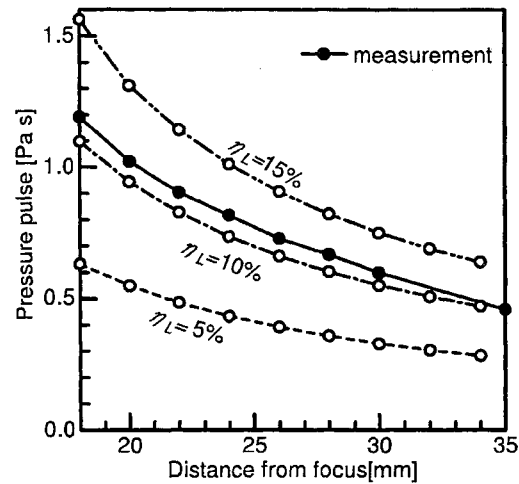


Fig. 10 Positive pressure pulse.

the energy consumed for dissociation and ionization in the fire-ball is neglected in the simulation. And the other is the possibility that some part of laser energy may be reflected or deflected by the plasma.

Figure 11 shows the variation of pressure, density and temperature profiles with interval of  $5\mu\text{s}$  from the laser termination  $t = 5\mu\text{s}$  to  $t = 30\mu\text{s}$ . As the wave propagates, its amplitude gradually decays. The negative pressure phase appears from  $t = 10\mu\text{s}$  to  $15\mu\text{s}$ . The pressure near the focus gradually recovers to the atmospheric pressure. (Fig.12) Finally, the pressure wave becomes a spherical acoustic wave and propagates in the undisturbed region.

Although the region behind the blast wave is homogeneously heated until  $t = 5\mu\text{s}$  in this simplified model, the boundary of high temperature region is already separated from the blast wave at

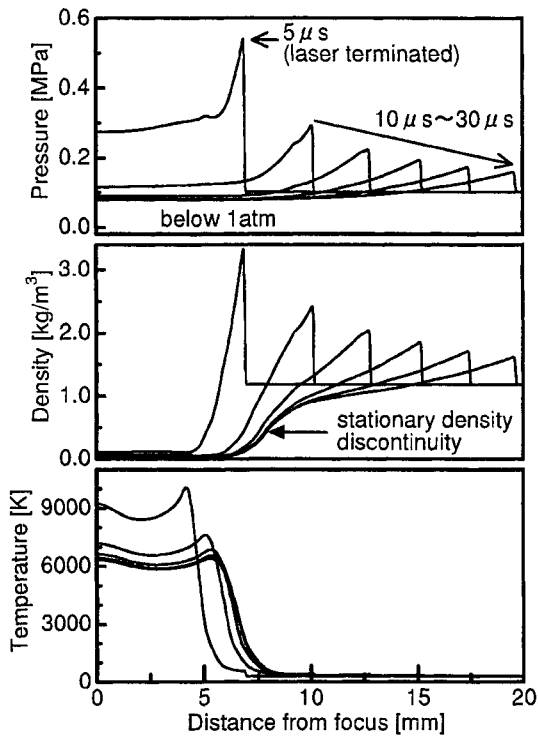


Fig. 11 Pressure, temperature and density profiles.

$t = 5\mu s$ . This is because the laser intensity is not high enough to maintain the laser supported detonation. After that, the high temperature region expands until its pressure drops to atmospheric pressure until  $15\mu s$ . Finally, the boundary of the high temperature region becomes stationary near  $r = 7\text{mm}$ . The temperature is kept at almost  $300\text{K}$  outside of this region. Therefore, if the receiver is to be located further than the boundary, heat conduction to the receiver would be negligibly small.

Figure 13 shows the history of the pressures on the receivers placed at  $r = 20\text{mm}$  and  $34\text{mm}$ . It contains positive and negative pressure phases. After the pressure rapidly rises up on the receiver by the reflection of incident shock, it decreases into the negative pressure phase and finally returns to atmospheric pressure. The negative pressure phase area increases proportionally to the distance from the focus.

The thrust impulse,  $I$ , is defined as a product of the time integration of  $p_{\text{rec}} - p_{\text{atm}}$  and the area of receiver. The  $p_{\text{rec}}$  is the pressure on the receiver.

$$I = \pi R_{\text{rec}}^2 \times \int (p_{\text{rec}} - p_{\text{atm}}) dt. \quad (6)$$

The thrust impulse is estimated separately according to the pressure phase. The positive impulse is defined as  $I_{\text{pos}} = \pi R_{\text{rec}}^2 \times \int_{t_0}^{t_1} (p_{\text{rec}} - p_{\text{atm}}) dt$ , the negative is  $I_{\text{neg}} = \pi R_{\text{rec}}^2 \times \int_{t_1}^{t_2} (p_{\text{rec}} - p_{\text{atm}}) dt$ , and the net is  $I_{\text{net}} = \pi R_{\text{rec}}^2 \times \int_{t_0}^{t_2} (p_{\text{rec}} - p_{\text{atm}}) dt$ .  $t_0$  is

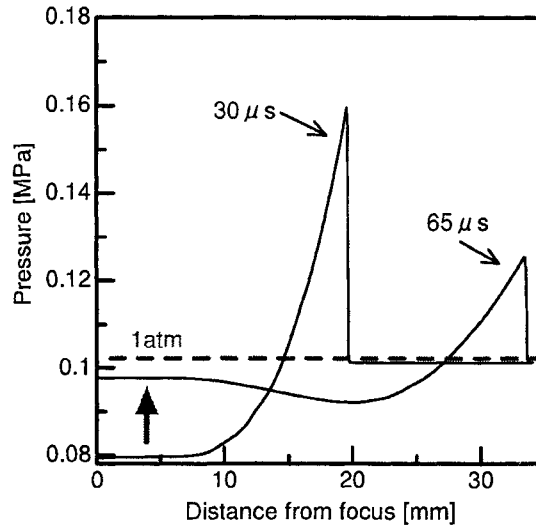


Fig. 12 Transition to a weak shockwave.

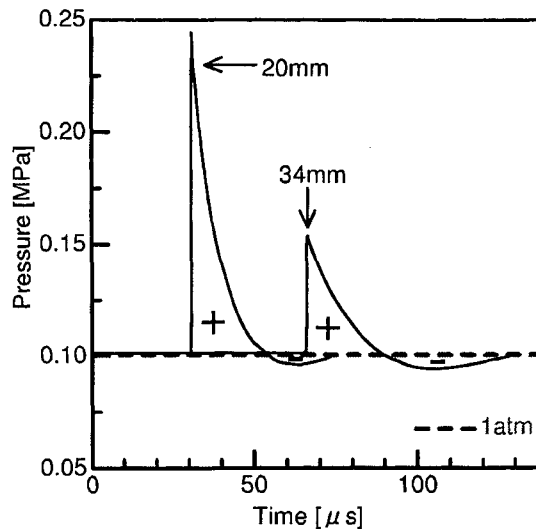


Fig. 13 Pressure history on the wall.

the time when the blast wave arrives at the receiver,  $t_1$  is the time when the negative pressure phase appears, and  $t_2$  is the time when the pressure recovers to the atmospheric pressure. The thrust impulses are shown in Fig.14.  $|I_{\text{neg}}|$  is the absolute value of the negative impulse. The positive impulse increases in proportion to the distance in the range from  $r = 18\text{mm}$  to  $34\text{mm}$ .

While the pressure decays inversely with  $R_{\text{rec}}$  in the far-field, the receiver area increases in proportion to  $R_{\text{rec}}^2$ . As a result, the positive impulse increases in proportion to  $R_{\text{rec}}$ . Since the negative impulse also increases with  $R_{\text{rec}}$ , the increases in both positive and negative impulse cancel out almost completely in the far-field.

In order to estimate the optimum location of receiver  $R_{\text{opt}}$ , the maximum impulse  $I_{\text{max}}$ , is calculated in several absorbed energy values from  $0.5\text{J}$

to 4.0J. Figure 15 shows  $R_{opt}$ ,  $I_{max}$ , and  $R_{limit}$  which is the limit position of expansion of the fire-ball. At the input energy of 1J, the maximum impulse of 1.1mNs is obtained on the receiver at  $r = 21\text{mm}$  apart from the focus.  $I_{max}$  increases in proportion to the absorbed energy at the slope of 1.1mNs per 1J.

Although  $R_{limit}$  increases with the absorbed energy,  $R_{opt}$  is far enough from  $R_{limit}$ . Consequently, the heat conduction to the receiver can be neglected in the far-field thruster.

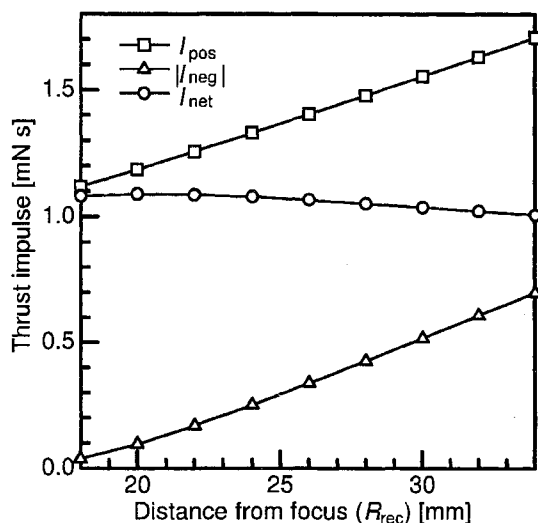


Fig. 14 Thrust impulse.

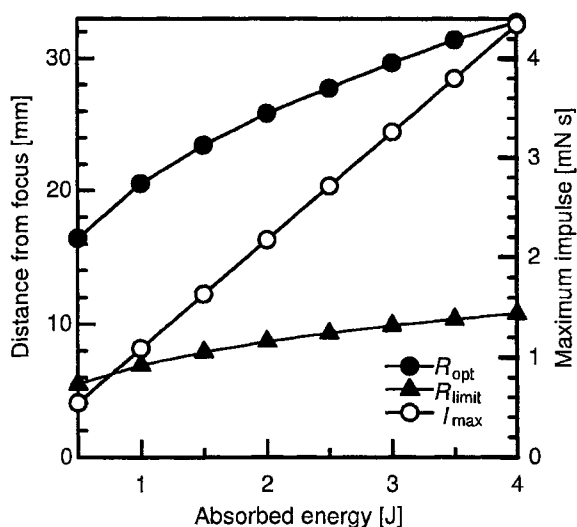


Fig. 15 Optimum receiver location and limit of expansion of fire ball, and maximum impulse, versus absorbed energy.

### SUMMARY

In the experiments, two density discontinuities were observed. One is expanding and the other is stationary after the laser irradiation. From the

simulation results, it was found that the former is a blast wave and the latter is an outer boundary of the fire-ball.

The computed and measured pressure profiles in the far-field show good agreement. Since the estimated net impulse hardly varies with the location of receiver, it is desirable to employ a small receiver in order to reduce the total weight of thruster and its aerodynamic drag, as long as the receiver never enters in contact with the fire-ball as  $r > R_{limit}$ .

Future research should precisely model the size of fire-ball as well as the thrust due to the nozzle expansion, aiming to establish the thruster scaling laws.

### REFERENCE

- [1] Myrabo, L.M., Messitt, D.G., and Mead, F.B., Jr., "Ground and Flight Tests of a Laser Propelled Vehicle," AIAA Paper 98-1001, Jan., 1998.
- [2] Wang, T-S., Cheng, Y-S., Liu, J., Myrabo, L.N., and Mead, F.B., Jr., "Performance Modeling of an Experimental Laser Propelled Lightcraft," AIAA Paper 00-2347, June, 2000.
- [3] Zel'dovich, Y.B., and Raizer, Y.P., "Physics of Shock waves and High-Temperature Hydrodynamic Phenomena," Academic Press, New York, 1966.
- [4] Ritzel, D.V., and Matthews, K., "An Adjustable Explosion-Source Model for CFD Blast Calculations," Proceedings of 21st International Symposium on Shock Waves, pp.97-102., Great Keppel Island, Australia, July 20-25, 1997.
- [5] Brode, H.L., "Numerical Solutions of Spherical Blast Waves," J. Appl. Phys., Vol.26, pp.766-775., 1955.
- [6] Shima, E., and Jounouchi, T., "AUSM Type Upwind Schemes," National Aerospace Laboratory in Japan, Special Publication, No.34., pp.7-12., 1997.
- [7] van Leer, B., "Toward the Ultimate Conservation Difference Scheme. IV, A New Approach to Numerical Convection," J. Comput. Phys., Vol.23, pp.276-299., 1977.
- [8] Geohegan, D.B., "Fast intensified-CCD photography of  $\text{YBa}_2\text{Cu}_3\text{O}_{7-x}$  laser ablation in vacuum and ambient oxygen," Appl. Phys. Lett., Vol.60, No.22, pp.2732-2734., 1992.